

This is the author's final, peer-reviewed manuscript as accepted for publication (AAM). The version presented here may differ from the published version, or version of record, available through the publisher's website. This version does not track changes, errata, or withdrawals on the publisher's site.

Combined Role of Biaxial Strain and Nonstoichiometry for the Electronic, Magnetic, and Redox Properties of Lithiated Metal-Oxide Films: The LiMn₂O₄ Case

Ivan Scivetti and Gilberto Teobaldi

Published version information

Citation: I Scivetti and G Teobaldi. Combined Role of Biaxial Strain and Nonstoichiometry for the Electronic, Magnetic, and Redox Properties of Lithiated Metal-Oxide Films: The LiMn₂O₄ Case. ACS Appl Mater Inter 13, no. 45 (2021): 54610-54619

DOI: [10.1021/acsami.1c18326](https://doi.org/10.1021/acsami.1c18326)

This document is the Accepted Manuscript version of a Published Work that appeared in final form in ACS Applied Materials & Interfaces, copyright © American Chemical Society after peer review and technical editing by the publisher. To access the final edited and published work see DOI above.

Please cite only the published version using the reference above. This is the citation assigned by the publisher at the time of issuing the AAM. Please check the publisher's website for any updates.

This item was retrieved from **ePubs**, the Open Access archive of the Science and Technology Facilities Council, UK. Please contact epublications@stfc.ac.uk or go to <http://epubs.stfc.ac.uk/> for further information and policies.

The Combined Role of Bi-Axial Strain and Non-Stoichiometry for the Electronic, Magnetic and Redox Properties of Lithiated Metal-Oxides Films: the LiMn₂O₄ Case

Ivan Scivetti^{1,2,*} and Gilberto Teobaldi^{2,3,4,†}

¹Scientific Computing Department, STFC UKRI, Daresbury Laboratory, WA4 4FS Warrington,
United Kingdom

²Stephenson Institute for Renewable Energy, Department of Chemistry, University of Liverpool,
L69 3BX Liverpool, United Kingdom

³Scientific Computing Department, STFC UKRI, Rutherford Appleton Laboratory, Harwell
Campus, OX11 0QX Didcot, United Kingdom

⁴School of Chemistry, University of Southampton, Highfield, SO17 1BJ Southampton, United
Kingdom

*Email: ivan.scivetti@stfc.ac.uk ; †Email: gilberto.teobaldi@stfc.ac.uk

Abstract. Understanding the interplay between strain and non-stoichiometry for the electronic, magnetic, and redox properties of LiMn_2O_4 films is essential for their development as Li-ion battery (LIB) cathodes, photo-electrodes, and systems for sustainable spintronics applications as well as for emerging applications that combine these technologies. Here, Density Functional Theory (DFT) simulations suggest that compressive strain increases the reduction drive of (111) LiMn_2O_4 films by inducing >1 eV upshift of the Valence Band edge. The DFT results indicate that, regardless of the crystallographic orientation for the LiMn_2O_4 film, bi-axial expansion increases the magnetic moments of the Mn-atoms. Conversely, bi-axial compression reduces them. For ferromagnetic films, these changes can be substantial and as large as over 4 Bohr magnetons per unit cell over the simulated range of strain (from -6% to +3%). The DFT simulations also uncover a compensation mechanism whereby strain induces opposite changes in the magnetic moment of the Mn and O atoms, leading to an overall constant magnetic moment for the ferromagnetic films. The calculated strain-induced changes in the atomic magnetic moments reflect modifications in the local electronic hybridization of both the Mn and O atoms, which in turn suggests strain-tunable, local chemical and electrochemical reactivity. Several energy-favored (110) and (111) ferromagnetic surfaces turn out to be half-metallic with minority spin band-gaps as large as 3.2 eV and compatible with spin-dependent electron-transport, and possible spin-dependent electrochemical and electrocatalytic properties. The resilience of the ferromagnetic, half-metallic states to surface non-stoichiometry and compositional changes invites exploration of the potential of LiMn_2O_4 thin-films for sustainable spintronics applications beyond state of the art, rare-earth metal based, ferromagnetic half-metallic oxides.

Keywords: LiMn_2O_4 , biaxial strain, non-stoichiometry, batteries, redox properties, ferromagnetism, half-metallicity, spintronics.

1. INTRODUCTION

Lattice strain can be used to tune the electronic properties of materials and thin-films, minimizing the risk of phase transformations and detrimental effects on structural integrity and functionality.^{1,2} The harnessing of lattice strain promises alternatives in the search for tailored materials to meet technological challenges, bypassing often expensive or hazardous synthetic approaches to modify the chemical composition of materials and manufacture nano-engineered interfaces.³ Controlled use of lattice strain has been successfully implemented and shown to be beneficial in fields as diverse as semiconductor electronics,⁴ topological insulators,⁵ photocatalysis,^{6,7} metal- and metal-oxide based catalysis and corrosion protection,⁸⁻¹¹ oxygen electro-catalysis and electrochemistry,^{1,2,12,13} as well as ion-diffusion in lithium-ion batteries (**LIBs**).^{14,15}

In spite of these advances, the interplay between lattice strain and non-stoichiometry in metal-oxide surfaces for the emerging electronic, magnetic and redox-chemistry properties remains overlooked. This has prevented the development of guidelines for combined use of strain and non-stoichiometry to tune the redox chemistry of metal-oxide surfaces *and/or* promote the emergence of bespoke electronic and magnetic surface properties. This situation is particularly unfortunate for LIBs,¹⁶ where control of the reactions at the electrode/electrolyte interface is essential for the stability of the electrode-electrolyte interphases (solid electrolyte interphase, **SEI**, at the anode, and cathode electrolyte interphase, **CEI**, at the cathode)^{17,18,19,20,21,22,23} that are critical for the performance and lifetime of devices. Such a knowledge gap also prevents rational, expedited progress in the fields of oxide-based photo-electro-catalysis,^{3,24,25} oxide-based sustainable spintronics,^{26,27,28} and, critical for the present study, at the interface between these areas of research and their focus on *different* chemical and physical properties of the *same* (or compositionally similar) oxides.

As hybrid technologies based on combination of diverse electrochemical, opto-electronic and magnetic functions for a given material begin to emerge,^{26,27,28,29} their optimization and uptake

require fundamental computational studies with an integrative, holistic approach to the combination and interplay of different materials properties. We believe this emerging class of hybrid applications also invites computational studies targeted at screening the material-specific dependence on intrinsic and extrinsic factors of the *interplay* between specific chemical and physical properties of interest.

To this end, here we use Density Functional Theory (**DFT**) to explore and quantify the interplay between bi-axial lattice strain and surface non-stoichiometry for the electronic, magnetic, and redox properties of an archetypal lithiated metal-oxide: spinel LiMn_2O_4 . LiMn_2O_4 is an alternative cathode material for high-power electromotive applications of future LIBs.³⁰ Despite the vast research in LiMn_2O_4 cathodes,³¹⁻³⁴ the reaction mechanisms at the surfaces of this material remain debated and poorly controlled, resulting in its degradation upon cycling and impeding its commercial uptake.³⁵

In recent years, the use of ultra-high vacuum epitaxial growth has benefited experimental research in surface chemistry and spintronics by enabling controlled manufacturing of relatively flat ultra-thin films with the desired composition, crystallographic phase and orientation.^{17,18,26,36, 37}

Epitaxial growth can also induce strain in thin-films by lattice misfit at the interface with the supporting substrate.³⁸ Experiments on LiMn_2O_4 thin-films grown over SrTiO_3 demonstrate that the film's (electro-)chemical properties are critically dependent on the crystallographic orientation.

Whereas electrolyte wetting of the (111) surface leads to CEI formation, wetting of the (110) facet induces dissolution of Mn^{+2} into the electrolyte, even at zero-voltage conditions i.e. in the absence of an externally applied voltage. The facet-dependent electrochemistry of LiMn_2O_4 films may also be relevant for electrochemically controlled, sustainable hybrid-spintronics applications. This new class of applications has been recently demonstrated using electrochemically induced ion-diffusion in sub-stoichiometric manganese oxides (MnO_x) films interfaced with molecular films under potentiostatic control.²⁷ These considerations provide further motivations for our interest in the

dependence of the magnetic properties of LiMn_2O_4 films on both strain and non-stoichiometry.

Finally, continuous progress in the synthesis and modification of piezoelectric thin-films³⁹⁻⁴² holds great promise for their use also as deposition substrate for functional films and *dynamic* external control of strain therein. Development and optimization of such approaches to dynamic property-tuning in functional films, possibly also in conjunction with electrochemical intercalation, self-evidently require understanding of the interplay between electrochemical and magnetic properties for a given material, which we start contributing here for LiMn_2O_4 films. We thus expect the present findings on the interplay between non-stoichiometry and strain for the electronic, magnetic and redox properties of LiMn_2O_4 films to be valuable for a wide readership with applicative interests in LIB-cathodes, (photo-)electro-catalysis and sustainable spintronics applications as well as in emerging hybrid technologies at the intersection between these currently minimally connected areas.

2. COMPUTATIONAL METHODS

Fully unconstrained, spin-polarized Density Functional Theory (DFT) calculations were carried out using the anisotropic (U-J) approach⁴³ with periodic boundary conditions (PBCs) and the projector-augmented wave method as implemented in the VASP program.^{44,45} Based on our previous work on vacuum-exposed LMO surfaces,³¹ we used the GGA-PW91 approximation⁴⁶ for the electronic exchange-correlation (XC) interaction, including the interpolation formula of Vosko et. al.,⁴⁷ with $U=6.2$ eV and $J=1.2$ eV anisotropic Hubbard corrections for the $3d$ orbitals of the Mn atoms.^{31,48} As benchmarked in Ref. 48, anisotropically (U-J) corrected GGA-like XC-functionals (as used here) can describe the magnetic properties and underpinning electronic hybridization in Mn-oxides with an accuracy comparable to that of hybrid DFT, resulting in semi-quantitative agreement between calculated and experimental results. The suitability of the adopted DFT+(U-J) approach in modeling strain-dependent semiconductor-to-metal transitions for LiMn_2O_4 slabs was validated against

screened hybrid-HSE06⁴⁹ results for the stoichiometric (110) slab. Owing to the increased computational cost of the HSE06 simulations in comparison to the DFT+(U-J) ones, these benchmarks were carried out on slabs of reduced thickness (56 atoms, 8 LiMn₂O₄ units arranged in 8 atomic layers). Based on recent benchmarking of the (overestimated) description of the band-gap for bulk LiMn₂O₄ by the standard HSE06 XC-functional with 25% Hartree-Fock (HF) mixing,⁵⁰ and following standard procedures for fine-tuning of the HF-mixing on experimental band-gaps,⁵¹ this validation was carried out with 10.5% (not 25%⁴⁹) HF-mixing. Such HF-mixing was tested to recover the experimental band-gap for bulk LMO (1.2 eV⁵⁰). The interested reader is referred to the Supporting Information (Section SI-6, Table S2) for further details.

Dispersion interactions were included via the van der Waals (vdW)-corrected DFT formalism with the parametrization proposed by Grimme,⁵² and a global scale factor equal to 0.7 for the PW91 exchange-correlation functional.

We assumed the LiMn₂O₄ crystal in its cubic phase, which is the phase observed for operational temperatures of LIBs. A vacuum buffer of at least 12 Å was included to avoid spurious interactions between opposite surfaces of the PBC-replicated slabs.

Electronic energies were converged within tolerances of 10⁻⁴ eV for a plane-wave energy cutoff of 550 eV. The 2D Brillouin zones were sampled using the Monkhorst-Pack scheme with 3x3 k-points for the (001) and (110) surfaces, whereas 2x4 k-points were used for the (111) surface. All atomic positions were relaxed until the ionic forces became lower than 0.03 eV/Å. Following previous research in reducible transition metal-oxides,^{53,54} Mn⁺⁴, Mn⁺³ and Mn⁺² sites were identified from the computed atomic magnetic moments.^{31,69}

All the simulated stoichiometric slabs were composed of 168 atoms (24 LiMn₂O₄ units), arranged in 24 atomic layers and with optimized thicknesses in the 2.66-2.84 nm range. These were checked to be sufficiently large to yield surface energies converged to within 0.01 J/m².³¹ To cancel the

inherent perpendicular dipole moment of these polar slabs, we applied the Tasker method⁵⁵ by transferring atoms between opposite surfaces of the slabs.³¹ All the slab models are symmetric along the z-axis, perpendicular to the surface (see Section SI-5). This symmetry condition ensures dipole-free slabs and excludes the need to apply dipole corrections. The procedures followed to build the non-stoichiometric slabs and to calculate their relative thermodynamic stability are detailed in the Supporting Information (Sections SI-8 and SI-9). We note that the present study is not focused in comparing the relative stability between different facets of the LiMn₂O₄ films. Instead, we are interested in epitaxially grown LiMn₂O₄ films, where the surface orientation of the film is determined by the crystallographic structure of the deposition substrate.¹⁸ Depending on the lattice misfit between the LiMn₂O₄ films and the deposition substrate, the films will be exposed to tensile or compressive strains as studied here. Finally, we note that the stoichiometric models of the (001), (110) and (111) slabs in Figs. 1-2 have the same number of atoms, which enables direct comparison of their relative energy, should the reader be interested in so doing. The same does not hold for the non-stoichiometric models in Figs. 3-4.

Following checks on the quantitatively negligible dependence of the strain-induced changes in atomic magnetic moments on the (projection or volume-integration) protocol used to integrate the spin-density (Section SI-7, Fig. S11), and unless otherwise stated, all the atomic magnetic moment were calculated by projection of the spin-density into the PAW-core using the default VASP PAW-projectors.

In the following, we define the bi-axial strain (epitaxial lattice misfit) as:

$$\varepsilon^{(i)}(s^{(i)}) = (s^{(i)} - s_0^{(i)})/s_0^{(i)},$$

where $s^{(i)}$ and $s_0^{(i)}$ correspond to the absolute value (module) of the two surface lattice vectors (i=1,2) of the strained and strain-free film, respectively. In this work, we assume that LiMn₂O₄ films form a coherent interface with its supporting substrate. Thus, the surface vectors of the strained film

($\vec{s}^{(1)}$ and $\vec{s}^{(2)}$) are the same as (or commensurate with) the surface vectors of the supporting substrate. This approximation is justified by the results of X-Ray Diffraction (XRD) experiments on air-exposed LiMn_2O_4 films supported by SrTiO_3 ,¹⁸ and excludes any possible change in the angle formed by the surface vectors for this type of systems. Although we do not include the supporting substrate explicitly in our simulations, we assume any bi-axial strain exerted over the film is such that it preserves the symmetry of the supporting substrate. The formulation in Section SI-13 demonstrates that this assumption is only valid when misfits $\varepsilon^{(1)}$ and $\varepsilon^{(2)}$ are the same, and this achieved when the surface vectors are scaled by the same factor, while keeping their orientations fixed.

3. RESULTS AND DISCUSSION

3.1 Stoichiometric (001), (110) and (111) LiMn_2O_4 surfaces

Here we focus on the (001), (110) and (111) facets of LiMn_2O_4 that are energetically favored in vacuo. We first consider stoichiometric surfaces in the canonical ensemble approximation.

In agreement with previous results for $\varepsilon=0$,³¹ we find that the lowest energy (001), (110) and (111) facets are Li [(001)-Li], Li-Mn-O [(110)-LMO] and Li terminated [(111)-Li], respectively (Figure 1). Once relaxed, (001)-Li and (110)-LMO contain the same amount of (high-spin) Mn^{+3} and (low-spin) Mn^{+4} sites in the slab. In contrast, (111)-Li hosts additional (very high-spin) sub-surface Mn^{+2} sites, introduced by the inverse spinel reconstruction (SI-4) and ensuing disproportionation.³¹

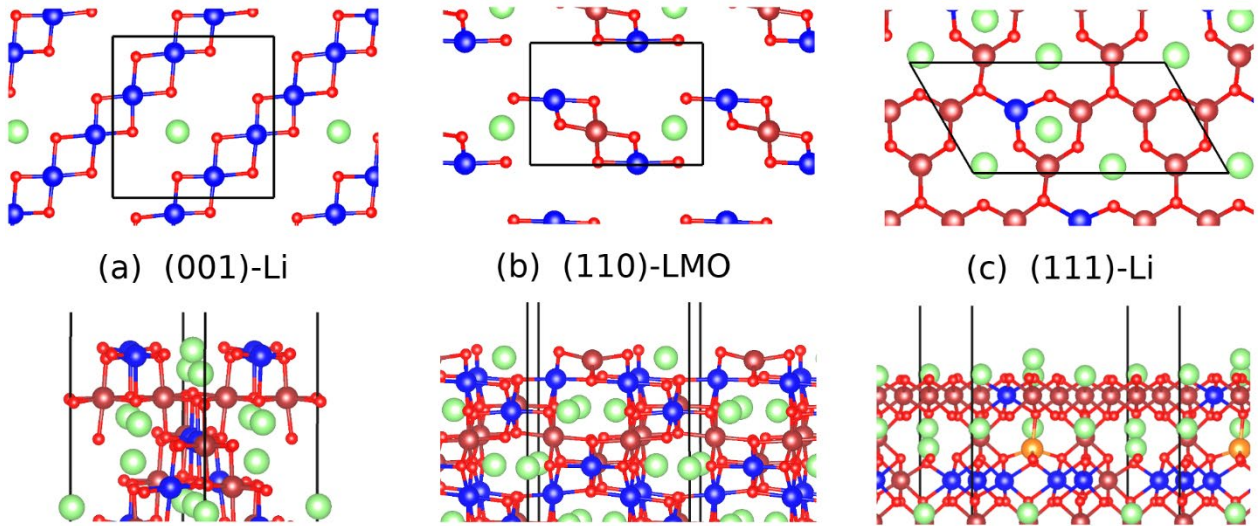


Figure 1. Top and side views of the optimized atomic structure for the lowest-energy, stoichiometric surfaces of LiMn_2O_4 : **(a)** (001)-Li, **(b)** (110)-LMO, **(c)** (111)-Li. For clarity, only the two outermost layers are displayed in the top views. The black lines mark the periodicity of the simulation cells. Mn^{+3} : blue, Mn^{+4} : maroon, Mn^{+2} : orange, O: red, Li: green.

Figure 2a shows the computed relative energies for the ferro-magnetic (**FM**) and anti-ferro-magnetic (**AFM**) ground-state solutions of the systems studied as a function of ϵ . For $\epsilon \geq 0$, and regardless of the magnetic ordering, (111)-Li is consistently favored (≥ 2 eV) over the other terminations. However, compression ($\epsilon < 0$) progressively reduces the (111)-Li favorability until $\epsilon \lesssim -2\%$, for which (001)-Li becomes the lowest energy surface. From being favored at zero-strain, (111)-Li turns into the highest-energy surface for $\epsilon \lesssim -4\%$. Regardless of the surface termination, FM ordering is systematically favored for tensile ($\epsilon > 0$) strain. Conversely, AFM ordering is favored by compression ($\epsilon \lesssim -2/-3\%$ depending on the surface, see also Figure S5). Strain can accordingly alter the relative energy of LiMn_2O_4 surfaces in both FM and AFM ordering, offering potential avenues to controlled engineering of magnetic ordering for LiMn_2O_4 thin films grown on suitably mismatched deposition substrates.

With the only exception of the AFM solution for (001)-Li, the atomic magnetic moments for the Mn and O atoms are strongly sensitive to strain (Figures 2c-d and S6-S8). Compression (expansion) is found to systematically decrease (increase) the magnetic moment of the Mn-atoms in the film, regardless of their oxidation state and overall magnetic ordering. As the rate of change with the applied strain is roughly the same for the AFM and FM solutions, the FM systems preserve their larger atomic magnetic moments by comparison to the AFM counterparts (Figures S6-S7). Notably, the simulations reveal a compensation mechanism whereby the changes in the magnetic moment of the O-atoms cancel those at the Mn-sites, leading to an overall constant slab-magnetic moment for the FM solutions across the whole range of ϵ studied. Based on this mechanism, strain could be used to separately tune the local electronic hybridization (oxidation state^{53,54,56}) and magnetism of the O- and Mn-sites at LiMn₂O₄ surfaces, potentially altering the local chemical reactivity towards those spin-polarized species that are inevitably present in multi-electron electro-photo-catalytic processes.^{1,2,6-13,57,58} As detailed in Section SI-7 (Fig. S11), we tested numerically that the calculated changes in atomic magnetic moments with strain do not depend on the method (PAW-projectors, radially truncated spherical harmonics, and Bader decomposition) used for atom-specific integration of the spin-density. The calculated changes should therefore be physical and not due to numerical artefacts.

Remarkably, whereas the FM and AFM solutions for (001)-Li and (111)-Li remain semiconducting for the whole range of ϵ studied, (110)-LMO in FM ordering becomes half-metallic for $\epsilon \lesssim -2\%$ (Figure S10). In the simulations, the minority-spin band-gap for this surface decreases linearly from 2.09 eV to 2.4 eV as the compressive strain is increased (in absolute value) from $\epsilon = -2\%$ to $\epsilon = -6\%$. These band-gap values are over 1.3 eV larger than the results for bulk cubic LiMn₂O₄ at the same level of theory (FM: 0.71 eV, AFM: 1.09 eV),³¹ suggesting that strain in thin films can be used to open band-gaps beyond the bulk limit.

Given the absence of any Self-Interaction Error correction on the O-atoms, the DFT+(U-J)

semiconductor-to-metal transition visible in Fig. S10 for the stoichiometric (110) slab in FM ordering for $\epsilon \leq -2\%$ requires additional validation, which we provide in the following using screened hybrid HSE06⁴⁹ results as reference.

Table S2 compares the calculated Kohn-Sham (direct) band-gaps for the stoichiometric (110) slabs at selected values of lattice misfit ϵ (-6%, 0%, +3%) and for different simulations set-ups. As indicated by the appearance of zero band-gaps (non-zero Density of States at the Fermi energy), simulation at DFT+(U-J) and HSE06 (10.5% and 12.5% HF mixing) level of both the DFT+(U-J) and HSE06 optimized geometries for compressive lattice misfits ($\epsilon=-6\%$) results in the appearance of (half-)metallic solutions. Whereas 10.5% HF mixing leads to a fully metallic solution, slight increase of HF-mixing to 12.5% results in a half-metallic system, as modeled at DFT+(U-J) level. The quantitative dependence of the calculated band-gaps on the HF-mixing is clearly both inevitable and unsurprising. However, the persistence of the compression-induced semiconductor to (half-)metal transition in both the DFT+(U-J) and screened hybrid DFT results provides confidence the computed effect should be qualitatively correct and, consequently, of potential significance in further developing LiMn₂O₄ films for applications that depend on electron- and/or spin-transport. With band-gaps for minority spin electrons in excess of 2.4 eV, the calculated half-metallicity of compressed (110)-LMO with FM ordering should result in strongly spin-dependent electron-transport properties. This is justified considering that the computed minority spin band-gaps for compressed LiMn₂O₄(110) films (≥ 2.4 eV) are actually larger than for a state of the art half-metallic ferromagnets such as La_{0.7}Sr_{0.3}MnO₃ (2 eV⁵⁹), a system heavily studied due to its spin-dependent electron transport properties. These results invite further research in compressed LiMn₂O₄ films for potential applications in spin-filtering devices²⁶⁻²⁸ or as an alternative to re-hybridization with organic molecules to generate half-metallicity in Mn-oxide films.²⁷

While the results of the simulations require experimental verification, the emergence of spin-

dependent electronic transport properties in compressed LiMn_2O_4 films also posits that the systems' electrochemistry will be affected. This because, pending “contact potential” considerations,^{20,21,22,60} application of external voltages smaller than the minority band-gap will inevitably populate only the majority spin bands resulting in surface excess charge of, at least initially, only one spin in contrast to the standard *diamagnetic* charging (same concentration of excess carriers for both electron spins).

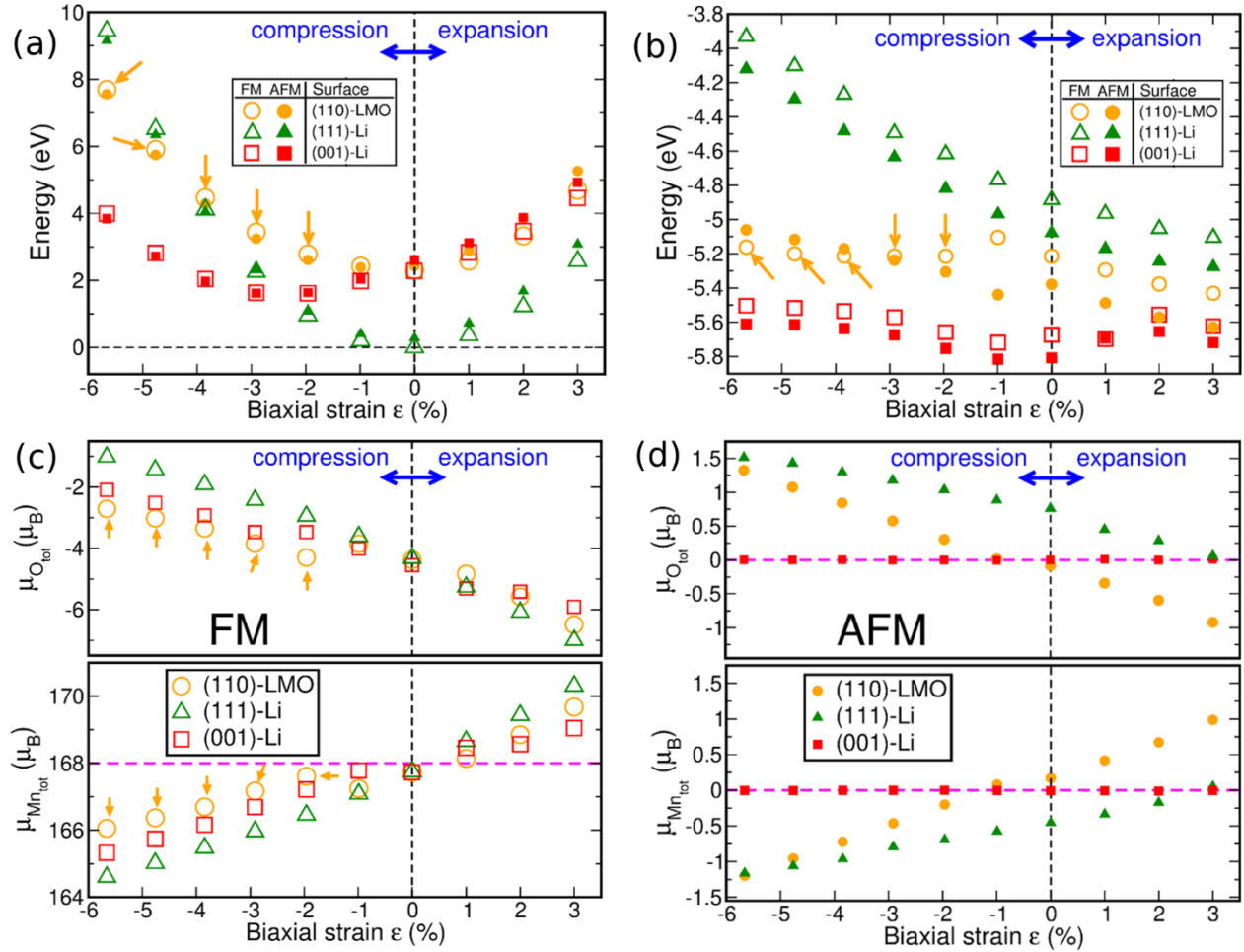


Figure 2. (a) Relative energies, (b) vacuum-aligned VBEs, and atom-resolved total magnetic moments (c-d) for the lowest energy stoichiometric LiMn_2O_4 surfaces as a function of bi-axial strain (ϵ) and (FM or AFM) magnetic ordering. The orange arrows point to the half-metallic solutions for compressed (110)-LMO. The pink horizontal lines in panels (c) and (d) mark the total magnetic moment of the slabs.

To investigate qualitatively the reduction drive of these systems, we align their Valence Band edge (VBE) to the vacuum level (Figure 2b). Although the vacuum-aligned VBEs in Fig. 2b neglect critical thermodynamics and kinetics effects due to dynamic relaxation at the solid-electrolyte interface and ensuing contact potential,^{20,21,22,60} they do allow direct comparison of the intrinsic energy drive to donate electrons for different systems.^{31,61,62} For the sake of clarity, we reiterate that, in the absence of values for the corresponding contact potential,^{20,60} the vacuum aligned VBEs (or workfunction for the metallic systems) cannot be immediately related to the absolute electrochemical potential of the LiMn₂O₄ films.

Moreover, although indicative of the energy drive to electron transfer (in vacuo),⁶² the calculated vacuum-aligned VBEs do not provide any quantitative information on the electrochemical mechanisms (kinetics included) of formation for passivation layers (CEI) on LiMn₂O₄ cathodes. In spite of all these limitations, the vacuum-aligned VBEs in Fig. 2b allow direct comparison of the combined role of surface-termination and strain in altering the energy position of the (adiabatic) electron-donor states of the systems. To the best of our knowledge, this aspect has not been previously considered in the literature on LiMn₂O₄ cathodes, although potentially relevant for future molecular-dynamics based studies of the thermodynamics and kinetics factors that need to be considered for quantitative understanding of the formation of passivation layers on battery electrodes.²⁰

For $\epsilon=0$, and regardless of the magnetic ordering, the VBE for (111)-Li is ~ 0.3 eV and ~ 0.8 eV higher than for (110)-LMO and (001)-Li, respectively, indicative of a larger reductive energy drive. The response of the VBE to compression turns out to be strongly facet-dependent. The VBEs remain practically unaltered for (001)-Li and (110)-LMO. Thus, the simulation indicates that application of strain should not be effective in tuning the reduction energy drive of the stoichiometric (001)-Li and (110)-LMO surfaces. In contrast, compression upshifts the VBE of (111)-Li by up to 0.4 eV ($\epsilon \approx 3\%$) and ≈ 1.0 eV ($\epsilon \approx 5.7\%$) with respect to the $\epsilon=0$ result. Thus,

compressive strain is calculated to enhance significantly the reduction drive of the stoichiometric (111)-Li surface. In general, the VBEs for the FM solutions are always slightly higher (≤ 0.2 eV) than for the AFM ones, indicating a slightly larger reduction drive for FM ordering. Conversely, we find the Conduction Band edge (**CBE**) for the FM solutions to be lower than for the AFM ones (Figure S9), leading to narrower FM band-gaps, independently of the strain (Figure S10). These trends are in line with earlier results for bulk LiMn_2O_4 at the same level of theory.^{31,48}

In both our previous³¹ and present simulations, we find that the VBEs for all the LiMn_2O_4 slabs are dominated by O(2p) states with smaller yet non-negligible contributions from Mn(3d) states. It thus follows that all the different LiMn_2O_4 slabs in Fig. 1 have their O(2p)-VBE in close proximity to the Fermi level. Based on a recent model for ethylene carbonate (EC) dissociation on the surfaces of both layered and rocksalts oxide surfaces (developed with no direct simulation of LiMn_2O_4 surfaces),¹⁹ all the terminations for LiMn_2O_4 films in Fig. 2b should exhibit a comparably strong energy drive to EC dissociation. However, such a hypothesis is in contrast with what was measured for differently oriented LiMn_2O_4 films exposed to a 1 M LiPF_6 electrolyte in an EC/diethyl carbonate (DEC) solution with molar ratio of 3:7.¹⁸ As a result of this discrepancy, and since different LiMn_2O_4 surfaces were not included in the development the O(2p)-band model in Ref. 19, we believe absolute alignment to a common reference (the vacuum level) for the VBE of the LiMn_2O_4 films presents advantages over the dissociation energy of EC for comparing the electron-donor levels of different surfaces as a function of strain.

However, it should be noted also that the vacuum-aligned VBEs in Fig. 2b do not allow any conclusion on the role of strain for the competition of different adsorption mechanisms of EC on LiMn_2O_4 films nor for the atomistic mechanism of formation for passivation layers on LiMn_2O_4 . To this end, and based on the markedly different response to strain for the O(2p)-dominated VBE of different LiMn_2O_4 surfaces in Fig. 2b, it remains to be assessed the extent to which and how strain may alter the competition between different adsorption pathways on this material and the

applicability of the O(2p)-model for strained LiMn_2O_4 cathodes. We hope our results and the present considerations will stimulate future work in the subject, which is clearly beyond the primary scope of this paper: the role of strain in tuning the interplay between electronic and magnetic properties for LiMn_2O_4 films.

As shown in Fig. 2b, the VBE for (111)-Li at $\varepsilon \approx 6\%$ is roughly 1 eV higher than for the unstrained systems at $\varepsilon = 0\%$, indicative of a substantially larger energy drive for electron transfer towards interacting molecules. This may play a role in the experimentally observed *zero-voltage* decomposition of the electrolyte on (111) surfaces.^{17,18} However, X-Ray Diffraction (XRD) experiments on air-exposed $\text{LiMn}_2\text{O}_4(111)$ films previous to electrolyte wetting reveal bulk-like lattice parameters for the films (7.32 ± 0.58 nm thick),¹⁷ which ultimately prevents direct comparison with our calculations on vacuum-exposed (2.66-2.84 nm thick) *strained* models. Clearly, DFT simulations of >7 nm thick slabs are impractically demanding, if not prohibitive. Therefore, further photoemission or electrochemical experiments on thinner LiMn_2O_4 film with XRD-confirmed strain would be needed to quantitatively validate the present results and their significance for the actual mechanisms of *zero-voltage* electrolyte decomposition on $\text{LiMn}_2\text{O}_4(111)$.

3.2 Non-stoichiometric (001), (110) and (111) LiMn_2O_4 surfaces

During the synthesis of LiMn_2O_4 films, the experimental conditions are inevitably adjusted to follow a given protocol, which causes deviations from the canonical ensemble, that is constant-particle, volume and temperature approximation we have assumed until now.³³ Thus, we next turn to simulations in the grand canonical ensemble to model a more realistic scenario where the system exchanges particles (atoms) with the environment, potentially resulting in non-stoichiometric surfaces, at constant chemical potential, volume and temperature. To this end, we quantify the relative stability of different LiMn_2O_4 surfaces as a function of strain *and* departure of the chemical

potentials of the constituent atoms ($\Delta\mu_\alpha$) from their standard reference values μ_α^S (α =Li, Mn, O). Details of the simulated surfaces are provided in Section SI-9. Due to the relatively small energy differences between the FM and AFM ordering of the stoichiometric surfaces (Figures 2 and S5), and to contain the computational cost, we limit this study to the FM solutions. For the analysis, we set $\Delta\mu_{Li}$ and $\Delta\mu_O$ as the two independent thermodynamic variables, with $\Delta\mu_{Mn}$ being defined by the stability condition of bulk LiMn_2O_4 (Sections SI-2 and SI-8).

Figure 3 reports the stability phase diagrams for different terminations of the (001), (110) and (111) facets at zero-strain ($\epsilon=0$) as a function of the changes in the chemical potential of the Li ($\Delta\mu_{Li}$) and O ($\Delta\mu_O$) atoms. As discussed in Section SI-2, the region of thermodynamic stability for bulk LiMn_2O_4 with respect to competing Mn-oxides is contained within the black polygons. The stoichiometric surfaces (*stoich*) analyzed in Figures 1 and 2 turn out to be energetically favored over a relatively limited region of the chemical-potential space. The computed phase diagrams for the (001) and (111) facets agree qualitatively with the findings of Ref. 33 at zero-strain. However, some deviations for the (110) facet appear. This reveals a non-negligible dependence of the results on the XC-functional (PW91 here, PBE in Ref. 33) and anisotropic (present case) or isotropic (in Ref. 33) Hubbard corrections, as typical for correlated Mn-oxides.^{31,48,63} For the interested reader, the Supporting Information (SI-10) provides an extensive analysis of these differences.

Notably, we find that the region of stability for each termination to be strongly sensitive to the applied strain ϵ , with the stoichiometric terminations of the (001) and (111) facets becoming unstable for substantial compression ($\epsilon < -4.76\%$), as indicated by their disappearance from the phase-stability diagrams (Figs. S16-S17). These results suggest that, depending on the strain introduced in LiMn_2O_4 thin-films, *different* non-stoichiometric surfaces could be engineered for the *same* protocol of film preparation. In principle, different strain in LiMn_2O_4 films may be introduced both *statically* by changing the epitaxial growth substrate and *dynamically* in the presence of piezoelectric properties for the growth substrate itself³⁹⁻⁴² or reversible electrochemical lithiation.³⁰⁻

³⁵ As these approaches are experimentally viable for metal-oxide thin-films,^{30-35,39-42} experimental validation of our results may be within reach and of potential significance for the diversified communities interested in functional films for LIB-electrodes, photo-electro-catalysis and sustainable spintronics applications.

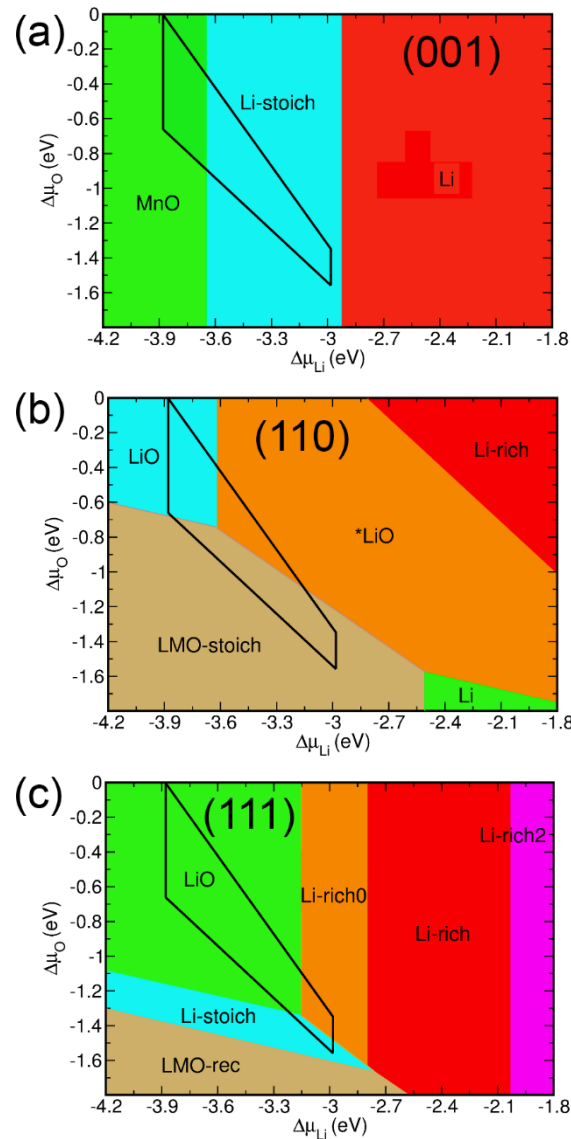


Figure 3. ($\Delta\mu_{Li}$, $\Delta\mu_O$) dependent stability phase diagrams for the different terminations of the (a) (001), (b) (110) and (c) (111) surfaces at zero-strain ($\epsilon=0\%$). The black polygon indicates the region of thermodynamic stability for bulk LiMn_2O_4 with respect to competing Mn-oxides (Figure S2). The fully relaxed atomic structures for each surface termination are shown in Figs S19 to S21.

Figure 4a-c report the calculated vacuum-aligned VBE as a function of ϵ for each of the energy favored terminations of the phase diagrams in Figure 3. The computed VBEs for the (001) and (110) facets are systematically below -5 eV, and practically independent of the applied strain. Conversely, the VBE of the (111) facets tends to increase with surface compression, the only exception being the *LMO-rec* termination whose VBE remains effectively constant regardless of the applied strain. Apart from the *LiO* termination, the VBE for all of the (111) terminations turns out to be above -4.0 eV for $\epsilon \lesssim -3\%$, indicative of a strongly enhanced reduction energy drive by comparison to the (110) and (001) facets (VBE < 5 eV), even in the presence of non-stoichiometry. As seen in Figure 4c, the VBEs of the *Li-rich* and *Li-rich2* terminations of the (111) surface are the highest regardless of the strain applied. These results suggest that in Li-rich conditions (Figure 3), as favored by strongly concentrated electrolytes, the energetically favored, Li-terminated (111) surfaces should be robustly reducing, which may promote *zero-voltage* reactions with the electrolyte. This result is in qualitative agreement with earlier computational results on Li-rich (111) surfaces of spinel $\text{Li}_7\text{Ti}_5\text{O}_{12}$.⁶⁴ The present simulations extend these earlier considerations by showing how the reduction energy drive for Li-terminated (111) surfaces of spinel LiMn_2O_4 can be further modulated by strain, with VBE change-rates as large as $\approx +0.2$ eV for 1% compression/expansion (*Li-rich2* in Figure 4c). The results in Figures S22-23 indicate that the calculated CBE for the semiconducting, non-stoichiometric LiMn_2O_4 surfaces show a rate of change with ϵ that is comparable to what observed in Fig. 4d-f for the VBEs. Thus, the calculated dependence of the systems' band-gap on the applied strain turns out to be rather weak.

In conjunction with impressive advances in the controlled preparation of both epitaxial metal-oxide thin-films^{17,18,36,38} and core-shell nanostructures,^{65,66} the strong sensitivity to strain of the VBE and CBE (thence redox chemistry drive) for the stoichiometric and non-stoichiometric LiMn_2O_4 surfaces (Figures 2, 4 and S22-23) motivates further research in strained LiMn_2O_4 films and zero-voltage formation of CEI precursors therein. The same dependence of the VBE and CBE of

LiMn₂O₄ surfaces on both strain and lithiation suggests also interesting opportunities in the development of strain- and lithiation-tailored LiMn₂O₄ films for photo-catalytic applications.^{3,24,25} We believe the calculated results and trends provide useful guidelines to prompt research in both of these directions.

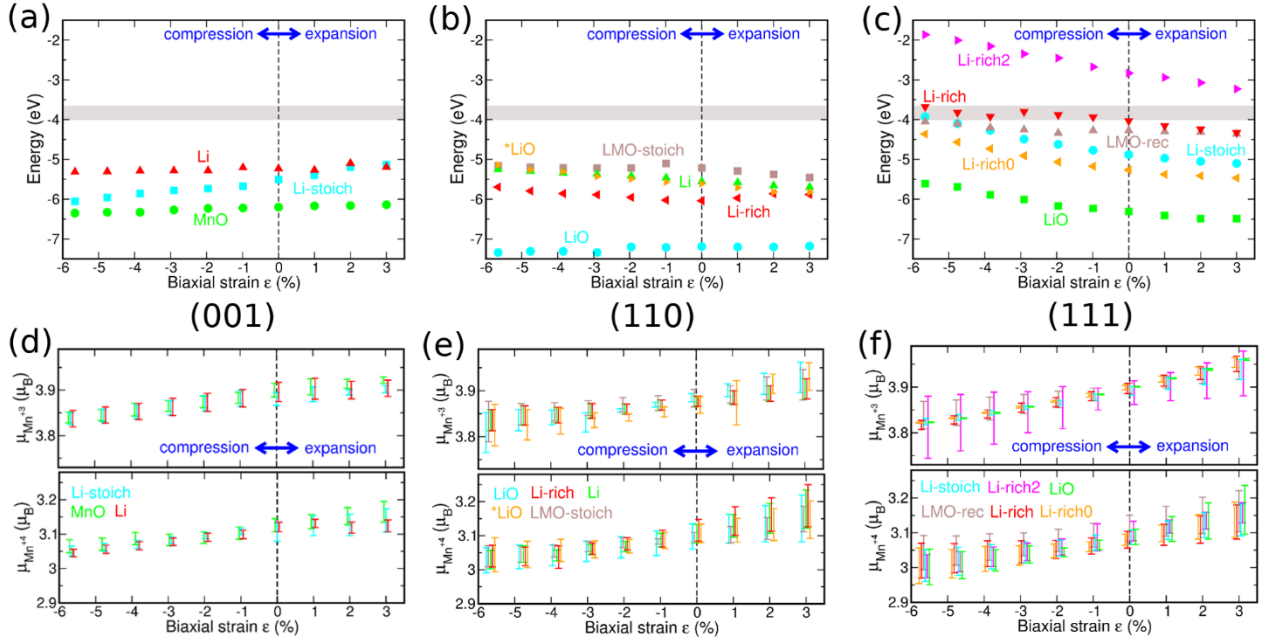


Figure 4. Vacuum-aligned VBEs (a-c) and atom-resolved average magnetic moments with standard deviation (d-f) for the energy-favored, stoichiometric and non-stoichiometric terminations of the (001) (a,d), (110) (b,e) and (111) (c,f) LiMn₂O₄ surfaces as a function of bi-axial strain (ϵ) in FM ordering.

Turning to the magnetic properties of non-stoichiometric LiMn₂O₄ surfaces, the results in Figure 4d-f indicate that compressive (tensile) strain leads to a decrease (increase) of the atomic magnetic moment for both low-spin Mn⁴⁺ and high-spin Mn³⁺ atoms also in the presence of non-stoichiometry. This trend is found consistently for all the (001), (110) and (111) orientations of the non-stoichiometric LiMn₂O₄ films. We find the computed *average* values to be very weakly

dependent on the given surface termination, indicative of a non-immediate role for the *surface* Li-content in tuning the local magnetic properties of LiMn_2O_4 . As for the stoichiometric models (Figure 2), the magnetic response of the O atoms to the application of strain is opposite to that of the Mn-atoms, leading to an overall strain-independent total magnetic moment for the simulated FM slabs. Notably, and in contrast with the result for the stoichiometric films (Fig. 2c), the simulations of the non-stoichiometric slabs reveal a non-negligible layer-dependence for the response of the atomic magnetic moments to the applied strain, which in turn generates an increased standard deviation for the calculated atomic moments in Fig. 4e-f. As detailed in Section SI-12 for the (111) *Li-rich2* slab (Figs. S25-27), such a response manifests in layer-dependent, local relaxed structures and oxidation states for specific subsets of atoms that are intermediate between the standard “+3” ($\sim 3.9 \mu_B$) and “+4” ($\sim 3.1 \mu_B$) results for bulk LiMn_2O_4 and its stoichiometric surfaces in Figs. 1-2. As evident across Figs. 4d-f, the inhomogeneity of the atomic response to strain appears to increase going from the (001) film to the (110) and (111) ones, and to be enhanced by Li-termination. Overall, these results indicates that although the surface Li-content does not significantly change the average atomic magnetic moments of the film, it does enhance the (atomic and layer) inhomogeneity of its response to the applied strain.

Also in the presence of non-stoichiometry, all the [(110) and (111)-*Li-rich2*] metallic surfaces of LiMn_2O_4 turn out to be half-metallic, with minority-spin band gaps strongly dependent on the applied strain (Figure 5). As per results in Figure S22, none of the (001) surface termination results in (half-)metallic solutions, within FM ordering. We find compressive ($\epsilon < 0$) and tensile ($\epsilon > 0$) strain to generally decrease and increase the minority spin band-gaps, respectively, albeit with exceptions such as the (111) *Li-rich2* and the (110) **LiO*, *LiO* and *Li-rich* terminations. Even the smallest minority-spin band-gap calculated [always larger than 1.4 eV for (110) *Li-rich* and $\epsilon \lesssim -5\%$] turns out to be substantially larger ($>30\%$) than for bulk FM (0.71 eV) or AFM (1.09 eV) LiMn_2O_4 at the same level of theory.³¹ These results indicate that, even in the presence of

substantial non-stoichiometry, strain in LiMn_2O_4 thin-films can yield energy-favored (Figure S5), robust half-metallicity with minority spin band-gaps beyond the bulk value. These findings in turn point to the possibility of strain-mediated strategies to introduce markedly spin-dependent electron-transport properties in LiMn_2O_4 films, likely to affect both the surface electrochemistry and the accumulation of spin-polarized, surface excess charge.²⁷

The persistence of half-metallic states in the non-stoichiometric (110) and (111) LiMn_2O_4 films indicates this property is rather robust with respect to (surface) compositional changes and, potentially, short-range disorder as recently observed at room-temperature for lithium-free, sub-stoichiometric Mn-oxides.²⁷ Given the well-known fragility of ferromagnetic half-metallic oxides to compositional changes and disorder,^{59,67-70} the present results point to strained LiMn_2O_4 films as a potential alternative system for spin-filtering applications that require robust ferromagnetism and half-metallicity. The absence of rare-earth metals in LiMn_2O_4 , in contrast to state of the art ferromagnetic half-metallic oxides,^{59,67-70} suggests further potential benefits in terms of sustainability,²⁸ thence motivation for further research into this subject.

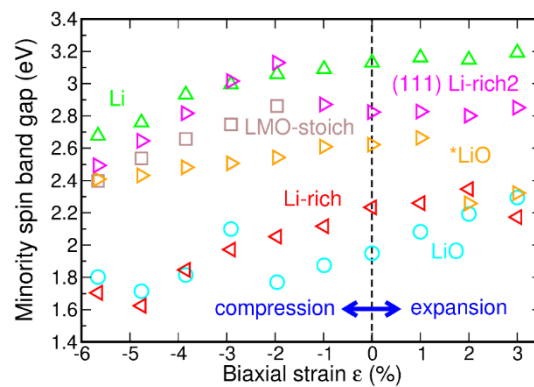


Figure 5. Calculated minority-spin band-gap for the half-metallic (111) *Li-rich2* and (110) terminations of LiMn_2O_4 as a function of bi-axial strain (ϵ). The (110) *LMO-stoich* termination becomes semiconducting for $\epsilon > -2\%$.

4. CONCLUSIONS

DFT+(U-J) simulations of the energy favored, stoichiometric and non-stoichiometric LiMn_2O_4 surfaces for different FM and AFM ordering in the presence of bi-axial strain reveal a marked (up to over 1 eV) increase in the reduction energy drive of the (111) terminations upon surface compression. This response could be further explored towards the design of new strategies to zero-voltage CEI-precursors for LiMn_2O_4 LIB-cathodes as well as strain-mediated engineering of LiMn_2O_4 band-edges for photo-electro-catalytic applications. The simulations indicate that, regardless of the FM or AFM ordering, the magnetic moment of the Mn-atoms increases (decrease) with application of tensile (compressive) strain. The simulations uncover a compensation mechanism whereby strain induces opposite changes in the magnetic moment of the Mn- and O-atoms, leading to an overall constant magnetic moment for FM slabs. This mechanism is observed in each of the systems studied apart from the AFM (001) Li-terminated surface, which indicates weak dependence on the crystallographic orientation of the film and its non-stoichiometry. These results are not affected by the specific method used to integrate the spin-density around atoms, which suggests the effect should be physical. Notably, several stoichiometric and non-stoichiometric (110) LiMn_2O_4 surfaces, and one non-stoichiometric (111) surface, turn out to be both ferromagnetic and half-metallic with a minority-spin band-gaps strongly sensitive to strain and up to over 2 eV (~200%) larger than for bulk LiMn_2O_4 , even in the absence of strain. Such values of minority spin band-gap are comparable with state of the art half-metallic ferromagnets based on oxides of rare earth metals. This in turn suggests markedly spin-dependent electron-transport properties that may affect also the electro-chemical and electro-catalytic reactions-mechanisms of the systems. The strong resilience of the calculated ferromagnetic half-metallic states to compositional changes (non-stoichiometry) suggests it may be rewarding to further explore the potential of strained LiMn_2O_4 (110) thin-films for sustainable spintronics applications, starting from, but not limited to, spin-filtering and spin-storage as recently measured for lithium-free Mn-oxides.²⁷

Associated Content.

Supporting Information

The Supporting Information, containing supplementary methods and results, is available free of charge at XXXX

Computational details for bulk LiMn_2O_4 calculations (SI-1); Stability of bulk LiMn_2O_4 (SI-2); Bulk LiMn_2O_4 response to bi-axial strain (SI-3); $\text{LiMn}_2\text{O}_4(111)$ inverse spinel reconstruction (SI-4); Symmetry restrictions in the simulation of the LiMn_2O_4 slabs (SI-5); Supplementary results for the relative energy, electronic and magnetic properties of the stoichiometric LiMn_2O_4 surfaces (SI-6); Spin-density integration to compute atomic magnetic moments (SI-7); Thermodynamic stability of LiMn_2O_4 surfaces: Theory (SI-8); Models of the non-stoichiometric LiMn_2O_4 surfaces (SI-9); Thermodynamic stability of non-stoichiometric LiMn_2O_4 surfaces: Results (SI-10); Strain-dependence of the VB and CB edges for the non-stoichiometric LiMn_2O_4 surfaces (SI-11); Supplementary results for the magnetic properties of non-stoichiometric LiMn_2O_4 surfaces (SI-12); Bi-axial strain (epitaxial lattice misfit): definitions (SI-13).

Author Contributions. GT developed the original research concept that was eventually expanded in collaboration with IS. Both authors analyzed jointly the results of the DFT (hybrid DFT) simulations that were executed by IS (GT). The manuscript was jointly written by both authors.

Notes. The authors declare no competing financial interest.

Acknowledgements

This work was supported by the EU FP7 project SIRBATT (contract no. 608502) and EPSRC UK (EP/I004483/1 and EP/S031081/1). This work made use of the HPC Wales, N8 (EPSRC UK EP/K000225/1), STFC Scientific Computing Department's SCARF, and ARCHER (via the UKCP Consortium, EPSRC UK EP/P022189/2) High-Performance Computing facilities. We are grateful to Stefano Passerini, Masaaki Hirayama, Miguel Angel Muñoz, Khang Hoang, Oscar Cespedes and Joshua Elliott for useful discussion and critical comments on the manuscript.

References

- (1) Yildiz, B. "Stretching" the Energy Landscape of Oxides—Effects on Electrocatalysis and Diffusion. *MRS Bulletin* **2014**, 39, 147.
- (2) Wen, K.; Lv, W.; He, W. Interfacial Lattice-Strain Effects on Improving the Overall Performance of Micro-Solid Oxide Fuel Cells. *J. Mater. Chem. A* **2015**, 3, 20031–20050.
- (3) Batzill, M. Fundamentals Aspects of Surface Engineering of Transition Metal Oxide Photocatalysts. *Energy Environ. Sci.* **2011**, 4, 3275-3286.
- (4) Wu, Y.; Chew, A. R.; Rojas, G. A.; Sini, G.; Haugstad, G.; Belianinov, A.; Kalinin, S.V.; Li, H.; Risko, C.; Brédas, J-L; Salleo, A.; Frisbie, C. D.;. Strain Effects on the Work Function of an Organic Semiconductor. *Nat. Commun.* **2016**, 7, 10270.
- (5) Lui, Y; Li, Y. Y.; Rajput, S.; Gilks, D.; Lari, L.; Galindo, P. L.; Weinert, M.; Lazarov, V. K.; Li, L. Tuning Dirac States by Strain in the Topological Insulator Bi₂Se₃. *Nat. Phys.* **2014**, 10, 294–299.
- (6) Cao, T.; Wang, D.; Geng, D-S.; Liu, L-M.; Zhao, J. A Strain or Electric Field Induced Direct Bandgap in Ultrathin Silicon Film and its Application in Photovoltaics or Photocatalysis. *Phys. Chem. Chem. Phys.* **2016**, 18, 7156–7162.
- (7) Feng, J.; Qian, X.; Huang, C-W.; Li, J. Strain-Engineered Artificial Atom as a Broad-Spectrum

Solar Energy Funnel. *Nat. Photonics* **2012**, 6, 866-872.

- (8) Pratt, A.; Lari, L.; Hovorka, O.; Shah, A.; Woffinden, C.; Tear, S. P.; Binns, C.; Kröger, R. Enhanced Oxidation of Nanoparticles Through Strain-Mediated Ionic Transport. *Nat. Mater.* **2014**, 13, 26-30.
- (9) Wang, S. D.; Li, W. Strain-Induced Changes in Electronic Structures and Work Function for (001), (110) and (111) of AlCu₃. *Physica B* **2011**, 406, 4046–4051.
- (10) Zhong, K.; Xu, G.; Zhang, J-M; Huang, Z. Effects of Strain on Effective Work Function for Ni/HfO₂ Interfaces. *J. Appl. Phys.* **2014**, 116, 063707.
- (11) Amakawa, K.; Sun, L.; Guo, C.; Hävecker, M.; Kube, P.; Wachs, I. E.; Lwin, S.; Frenkel, A. I.; Patlolla, A.; Hermann, K.; Hermann, K.; Schlögl; Trunschke, A. How Strain Affects the Reactivity of Surface Metal Oxide Catalysts. *Angew. Chem. Int. Ed.* **2013**, 52, 13553–13557.
- (12) Kim, S.; Choi, S. J.; Zhao, K.; Yang, H.; Gobbi, G.; Zhang, S.; Li, J. Electrochemically Driven Mechanical Energy Harvesting. *Nat. Commun.* **2016**, 7, 10146.
- (13) Muralidharan, N.; Carter, R.; Oakes, L.; Cohn, A. P.; Pint, C. L. Strain Engineering to Modify the Electrochemistry of Energy Storage Electrodes. *Sci. Rep.* **2016**, 6, 27542.
- (14) Tealdi, C.; Heath, J.; Islam, M. S. Feeling the Strain: Enhancing Ionic Transport in Olivine Phosphate Cathodes for Li- and Na-ion Batteries Through Strain Effects. *J. Mater. Chem. A* **2016**, 4, 6998.
- (15) Jia, M.; Wang, H.; Sun, Z.; Chen, Y.; Guo, C.; Gan, L. Exploring Ion Migration in Li₂MnSiO₄ for Li-Ion Batteries Through Strain Effects. *RSC Adv.* **2017**, 7, 26089.
- (16) Tarascon, J. M.; Armand, M. Building Better Batteries. *Nature* **2008**, 451, 652-657.
- (17) Hirayama, M.; Sonoyama, N.; Ito, M.; Minoura, M.; Mori, D.; Yamada, A.; Tamura, K.; Mizuki, J.; Kanno, R. J. Characterization of Electrode/Electrolyte Interface with X-Ray

- Reflectometry and Epitaxial-Film LiMn₂O₄ Electrode. *Electrochem. Soc.* **2007**, 154, A1065–A1072.
- (18) Hirayama, M.; Ido, H.; Kim, K.; Cho, W.; Tamura, K.; Mizuki, J.; Kanno, R. Dynamic Structural Changes at LiMn₂O₄/Electrolyte Interface during Lithium Battery Reaction. *J. Am. Chem. Soc.* **2010**, 132, 15268–15276.
- (19) Giordano, L.; Karayaylali, P.; Yu, Y.; Katayama, Y.; Maglia, M.; Lux, S.; Shao-Horn, Y. Chemical Reactivity Descriptor for the Oxide-Electrolyte Interface in Li-Ion Batteries. *J. Phys. Chem. Lett.* **2017**, 8, 3881–3887.
- (20) Leung, K. DFT Modelling of Explicit Solid–Solid Interfaces in Batteries: Methods and Challenges. *Phys. Chem. Chem. Phys.* **2020**, 22, 10412-10425.
- (21) Leung, K.; Rosy; Noked, M. Anodic Decomposition of Surface Films on High Voltage Spinel Surfaces—Density Function Theory and Experimental Study. *J. Chem. Phys.* **2019**, 151, 234713.
- (22) Østergaard, T. M.; Giordano, L.; Castelli, I. E.; Maglia, F.; Antonopoulos, B. K.; Shao-Horn, Y.; Rossmeisl, J. Oxidation of Ethylene Carbonate on Li Metal Oxide Surfaces. *J. Phys. Chem. C* **2018**, 122, 10442-10449.
- (23) Wang, A.; Kadam, S.; Li, H.; Shi, S.; Qi, Y. Review on Modeling of the Anode Solid Electrolyte Interphase (SEI) for Lithium-Ion Batteries. *Npj Comput. Mater.* **2018**, 4, 15.
- (24) Hoang, K. Understanding the Electronic and Ionic Conduction and Lithium Over-Stoichiometry in LiMn₂O₄ Spinel. *J. Mater. Chem. A* **2014**, 2, 18271-18280.
- (25) Maitra, U.; Naidu, B. S.; Govindaraj, A.; Rao, C. N. R. Importance of Trivalency and the e_g^1 Configuration in the Photocatalytic Oxidation of Water by Mn and Co Oxides. *Proc. Natl. Acad. Sci. U.S.A.* **2013**, 110, 11704–11707.
- (26) Cinchetti, M.; Dediu, V. A.; Hueso, L. E. Activating the Molecular Spinterface. *Nature Mater.*

2017, 16, 507–515.

- (27) Moorsom, T.; Rogers, M.; Scivetti, I; Bandaru, S.; Teobaldi, G.; Valvidares, M.; Flokstra, M.; Lee, S.; Stewart, R.; Prokscha, T.; Gargiani, P.; Stefanou, G. Ali, M.; Al Ma’Mari, F.; Burnell, G.; Hickey, B.J.; Cespedes, O. Reversible Spin Storage in Metal Oxide-Fullerene Heterojunctions. *Sci. Adv.* **2020**, 6, eaax1085.
- (28) Puebla, J.; Kim, J.; Kondou, K.; Otani, Y. Spintronic Devices for Energy-Efficient Data Storage and Energy Harvesting. *Comms. Mater.* **2020**, 1, 24.
- (29) Lee, A.; Vörös, M.; Dose, W. M.; Niklas, J.; Poluektov, O.; Schaller, R. D.; Iddir, H.; Maroni, V. A.; Lee, E.; Ingram, B.; Curtiss, L. A.; Johnson, C. S. . Photo-Accelerated Fast Charging of Lithium-Ion Batteries. *Nat. Commun.* **2019**, 10, 4946.
- (30) Ellis, B. L.; Lee, K. T.; Nazar, L. F. Positive Electrode Materials for Li-Ion and Li-Batteries. *Chem. Mater.* **2010**, 22, 691–714.
- (31) Scivetti, I.; Teobaldi, G. (Sub)surface-Promoted Disproportionation and Absolute Band Alignment in High-Power LiMn₂O₄ Cathodes. *J. Phys. Chem. C* **2015**, 119, 21358–21368.
- (32) Nakayama, M.; Taki, H.; Nakamura, T.; Tokuda, S.; Jalem, R.; Kasuga, T. Combined Computational and Experimental Study of Li Exchange Reaction at the Surface of Spinel LiMn₂O₄ as a Rechargeable Li-Ion Battery Cathode. *J. Phys. Chem. C* **2014**, 118, 27245–27251.
- (33) Warburton, R. E; Iddir, H.; Curtiss, L. A.; Greeley, J. Thermodynamic Stability of Low- and High-Index Spinel LiMn₂O₄ Surface Terminations. *ACS Appl. Mater. Interfaces* **2016**, 8, 11108–11121.
- (34) Chen, L.; Warburton, R. E.; Chen, K-S. ; Libera, J. A.; Johnson, C.; Yang, Z.; Hersam, M. C.; Greeley, J. P.; Elam, J. W. Mechanism for Al₂O₃ Atomic Layer Deposition on LiMn₂O₄ from In Situ Measurements and Ab Initio Calculations. *Chem.* **2018**, 4, 2418-2435.

- (35) Yonemura, M.; Kohigashi, T.; Yamada, A.; Sonoyama, N.; Kobayashi, H.; Kamiyama, T.; Kanno, R. Defect Structure of LiMn_2O_4 after High-Temperature Storage. *Electrochemistry* **2003**, 71, 1160–1161.
- (36) Ikuhara, Y. H.; Gao, X.; Huang, R.; Fisher, C. A. J.; Kuwabara, A.; Moriwake, H.; Kohama, K. Epitaxial Growth of LiMn_2O_4 Thin Films by Chemical Solution Deposition for Multilayer Lithium-Ion Batteries. *J. Phys. Chem. C* **2014**, 118, 19540–19547.
- (37) Moorsom, T.; Alghamdi, S.; Stansill, S.; Poli, E.; Teobaldi, G.; Beg, M.; Fangohr, H.; Rogers, M.; Aslam, Z.; Rogers, M.; Aslam, Z.; Ali, M.; Hickey, B. J.; Cespedes, O.. π -anisotropy: A nano-carbon route to hard magnetism. *Phys. Rev. B* **2020**, 101, 060408(R).
- (38) Santiso, J.; Roqueta, J.; Bagués, N.; Frontera, C.; Konstantinovic, Z.; Lu, Q.; Yildiz, B.; Martínez, B.; Pomar, A.; Balcells, L.; Sandiumenge, F. Self-Arranged Misfit Dislocation Network Formation upon Strain Release in $\text{La}_{0.7}\text{Sr}_{0.3}\text{MnO}_3/\text{LaAlO}_3(100)$ Epitaxial Films under Compressive Strain. *ACS Appl. Mater. Interfaces* **2016**, 8, 16823–16832.
- (39) Izyumskaya, N.; Alivov, Ya.; Cho, S. -J.; Morkoc, H.; Lee, H.; Kang, Y. -S. Processing, Structure, Properties, and Applications of PZT Thin Films. *Crit. Rev. Solid State Mater. Sci.* **2007**, 32, 111-202.
- (40) Fu, Y. Q.; Luo, J. K.; Nguyen, N. T.; Walton, A. J.; Flewitt, A. J.; Zu, X. T.; Li, Y.; McHale, G.; Matthews, A.; Iborra, E; Du, H.; Milne, W. I. Advances in Piezoelectric Thin Films for Acoustic Biosensors, Acoustofluidics and Lab-on-Chip Applications. *Prog. Mater. Sci.* **2017**, 89, 31-91.
- (41) Uppuluri, R.; Sen Gupta, A.; Rosas, A. S.; Mallouk, T.E. Soft Chemistry of Ion-Exchangeable Layered Metal Oxides . *Chem. Soc. Rev.* **2018**, 47, 2401-2430.
- (42) Li, L. J.; Miao, L.; Zhang, Z.; Pu, X. H.; Feng, Q.; Yanagisawa, K.; Fan, Y.; Fan, M. J.; Wen, P. H.; Hu, D. W. Recent Progress in Piezoelectric Thin Film Fabrication via the Solvothermal

Process. *J. Mater. Chem. A* **2019**, 7, 16046-16067.

- (43) Anisimov, V. I.; Zaanen, J.; Andersen, O. K. Band Theory and Mott Insulators: Hubbard U instead of Stoner I. *Phys. Rev. B* **1991**, 44, 943-954.
- (44) Kresse, G.; Furthmüller, J. Efficiency of Ab-Initio Total Energy Calculations for Metals and Semiconductors Using a Plane-Wave Basis Set. *Comput. Mater. Sci.* **1996**, 6, 15-50.
- (45) Kresse, G.; Joubert, D. From Ultrasoft Pseudopotentials to the Projector Augmented-wave Method. *Phys. Rev. B* **1999**, 59, 1758-1775.
- (46) Wang, Y.; Perdew, J. P. Correlation Hole of the Spin-Polarized Electron Gas, with Exact Small-Wave-Vector and High-Density Scaling. *Phys. Rev. B* **1991**, 44, 13298-13307.
- (47) Vosko, S. H.; Wilk, L.; Nusair M. Accurate Spin-Dependent Electron Liquid Correlation Energies for Local Spin Density Calculations: a Critical Analysis. *Can. J. Phys.* **1980**, 58, 1200-1211.
- (48) Tompsett, D. A.; Middlemiss, D. S.; Islam, M. S. Importance of Anisotropic Coulomb Interactions and Exchange to the Band Gap and Antiferromagnetism of β -MnO₂ from DFT+U. *Phys. Rev. B* **2012**, 86, 205126.
- (49) Heyd, J.; Scuseria, G. E. Erratum: "Hybrid Functionals Based on a Screened Coulomb Potential" [*J. Chem. Phys.* 118, 8207 (2003)]. *J. Chem. Phys.* **2006**, 124, 219906.
- (50) Eckhoff, M.; Blöchl, P. E.; Behler, J. Hybrid Density Functional Theory Benchmark Study on Lithium Manganese Oxides. *Phys. Rev. B* **2020**, 101, 205113.
- (51) He, J.; Franchini, C. Screened Hybrid Functional Applied to 3d⁰→3d⁸ Transition-Metal Perovskites LaMO₃ (M = Sc–Cu): Influence of the Exchange Mixing Parameter on the Structural, Electronic, and Magnetic properties. *Phys. Rev. B* **2012**, 86, 235117.
- (52) Grimme, S. Semiempirical GGA-type Density Functional Constructed with a Long-Range Dispersion Correction. *J. Comput. Chem.* **2006**, 27, 1787–1799.

- (53) Raebiger, H., Lany, S.; Zunger, A. Charge Self-Regulation Upon Changing the Oxidation State of Transition Metals in Insulators. *Nature* **2008**, 453, 763-766.
- (54) Jansen, M.; Wedig, U. A Piece of the Picture - Misunderstanding of Chemical Concepts. *Angew. Chem. Int. Ed.* **2008**, 47, 10026-10029.
- (55) Tasker, P. W. The Stability of Ionic Crystal Surfaces. *J. Phys. C* **1979**, 12, 4977-4984.
- (56) Rousseau, R.; Glezakou, V; Selloni, A. Theoretical Insights into the Surface Physics and Chemistry of Redox-Active Oxides. *Nat. Rev. Mater.* **2020**, 5, 460–475.
- (57) Garcés-Pineda, F. A.; Blasco-Ahicart, M.; Nieto-Castro, D.; López, N. ;Galán-Mascarós, J. R. Direct Magnetic Enhancement of Electrocatalytic Water Oxidation in Alkaline Media. *Nat. Energy* **2019**, 4, 519-525.
- (58) Ghosh, S.; Bloom, B. P.; Lu, Y.; Lamont, D.;Waldeck, D. H. Increasing the Efficiency of Water Splitting through Spin Polarization Using Cobalt Oxide Thin Film Catalysts. *J. Phys. Chem. C* **2020**, 124, 22610–2261.
- (59) Katsnelson, M. I.; Irkhin, V. Yu.; Chioncel, L.; Lichtenstein, A. I.; de Groot, R. A. Half-Metallic Ferromagnets: From Band Structure to Many-Body Effects. *Rev. Mod. Phys.* **2008**, 80, 315-378.
- (60) Trasatti, S. The Absolute Electrode Potential: an Explanatory Note (Recommendations 1986). *J. Electroanal. Chem. Interf. Electrochem.* **1986**, 209, 417.
- (61) Etxebarria, A.; Koch, S. L.; Bondarchuk, A.; Passerini, S.; Teobaldi, G.; Muñoz-Márquez, M. A. Work Function Evolution as Li Anode Stability Parameter. *Adv. Energy Mater.* **2020**, No. 2000520.
- (62) Koopmans, T. Über die Zuordnung von Wellenfunktionen und Eigenwerten zu den einzelnen Elektronen eines Atoms. *Physica* **1934**, 1, 104–113.
- (63) Tompsett, D. A.; Islam, M. S. Surfaces of Rutile MnO₂ Are Electronically Conducting,

Whereas the Bulk Material Is Insulating. *J. Phys. Chem. C* **2014**, 118, 43, 25009–25015.

- (64) Morgan, B. J.; Carrasco, J.; Teobaldi, G. Variation in Surface Energy and Reduction Drive of a Metal Oxide Lithium-Ion Anode with Stoichiometry: a DFT Study of Lithium Titanate Spinel Surfaces. *J. Mater. Chem. A* **2016**, 4, 17180–17192.
- (65) Xia, X.; Tu, J.; Zhang, Y.; Wang, X.; Gu, C.; Zhao, X.; Fan, J. F. High-Quality Metal Oxide Core/Shell Nanowire Arrays on Conductive Substrates for Electrochemical Energy Storage, *ACS Nano* **2012**, 6, 5531.
- (66) Lu, W.J.; Guo, X. T.; Luo, Y. Q.; Li, Q.; Zhu, R. M.; Pang, H. Core-shell Materials for Advanced Batteries. *Chem. Eng. J.* **2019**, 355, 208-237.
- (67) Coey, J. M. D; Chien, C. L. Half-Metallic Ferromagnetic Oxides. *MRS Bulletin* **2003**, 29, 720-724.
- (68) Coey, J. M. D; Sanvito, S. Magnetic Semiconductors and Half-Metals. *J. Phys. D: Appl. Phys.* **2004**, 37, 988-993.
- (69) Saloaro, M.; Hoffmann, M.; Adeagbo, W. A.; Granroth, S.; Deniz, H.; Palonen, H.; Huhtinen, H.; Majumdar, S.; Laukkanen, P.; Hergert, W.; Ernst, A.; Paturi, P. Toward Versatile Sr₂FeMoO₆-Based Spintronics by Exploiting Nanoscale Defects. *ACS Appl. Mater. Interfaces* **2016**, 8, 20440–20447.
- (70) Manna, K.; Sun, Y.; Muechler, L.; Kubler, J.; Felser, C. Heusler, Weyl and Berry. *Nature Rev. Mater.* **2018**, 3, 244-256.

For Table of Contents Only

